# Fabrication and characterization of *c*-Si/porous-Si/CdS/$Zn_xCd_{1-x}O$ heterojunctions for applications in nanostructured solar cells

Huseyn M Mamedov,*[1] Mustafa Muradov[1], Zoltan Konya[2], Akos Kukovecz[2], Krisztian Kordas[3], Syed Ismat Shah[4], Vusala J Mamedova[1], Khumar M Ahmedova[1], Elgun B Tagiyev[1], Vusal U Mamedov[1]

[1]*Baku State University, Z.Khalilov str., 23, Baku, Azerbaijan, Az1148*
[2]*University of Szeged, Dugonicstér 13, Szeged, Hungary, Szeged 6720*
[3]*Microelectronics Research Unit, University of Oulu, P.O.Box 4500, 90570, Oulu, Finland*
[4]*University of Delaware, 208 DuPont Hall, Newark, DE 19716, USA*

Received August 08, 2018; accepted September 07, 2018; published September 30, 2018

**Abstract**—Solar cells based on *c*-Si/porous-Si/CdS/$Zn_xCd_{1-x}O$ heterojunctions were synthesized by depositing CdS films on c-Si/porous-Si (PS) substrates by electrochemical deposition (ED). PS layers with a systematically varied pore diameter (8÷45nm) and were fabricated on p-type *c*-Si wafers using electrochemical etching. The window layers of $Zn_xCd_{1-x}O$ with several Zn concentrations ($x$=0.2; 0.4; 0.5 and 0.6) were also deposited on the CdS buffer layers by ED. The photoelectrical properties of heterojunctions were studied as functions of PS pore size and Zn content in $Zn_xCd_{1-x}O$. The optimal pore size and Zn contents were found to be 10nm and $x$=0.6, respectively. These yielded a solar cell sample exhibiting an efficiency of 9.9%, the maximum observed in this study.

It is generally known that the surface modification of the silicon wafer plays a major role in the sensitivity enhancement of a silicon solar cell [1-2]. Nanostructured porous silicon (PS) has emerged as an attractive material in the field of photoelectronics due to its broad band gap, wide optical transmission range, favorable absorption spectrum and surface texture. The surface roughness and low effective refractive index, which can reduce reflection losses of sunlight radiation, are the primary benefits offered by PS over *c*-Si [3-8]. A significant difference in the lattice constants of silicon and CdS (about 7%) stimulates the formation of surface states at interface. A highly porous PS layer can enhance the efficiency of solar cells by increasing light trapping in the active region [9], solves the lattice mismatches problem, and surface reflection is also corrected due to the refractive index of silicon as reported by several other authors [10-14].

ZnO and its ternary cadmium alloys ($Zn_xCd_{1-x}O$) are important semiconductor materials that are used in solar cells [15], light-emitting diodes [16], and other optoelectronic devices [17].

In the present study the p-type *c*-Si substrates (1.5 and 2.5 Ohm·cm resistivity and 0.2 mm thick) were cleaned before etching by rinsing with acetone, ethanol and dilute (10%) HF acid. The anodization of the *c*-Si substrate surface was carried out in a Teflon-lined chamber equipped with a platinum cathode. Hydrofluoric (HF) acid:ethanol (1:1) was used for the formation of porous silicon. The anodization voltage, current density and anodization time were (20; 25; 30)V, (50; 60; 70)mA/cm$^2$ and 1÷30min, respectively. The thickness of the PS layer was 250nm.

After the PS layer formation, samples were immersed into acetone and ethyl alcohol, dried in flowing $N_2$ and placed into an electrochemical bath for the deposition of CdS films. CdS films were electrodeposited onto *c*-Si/PS substrates at 80°C from an aqueous solution containing cadmium (0.2M $CdCl_2$) and sodium (0.05 M $Na_2S_2O_3$) salts (99.5% salt purity). The pH was changed from 5 up to 6 by using HCI. Depending on the deposition time and substrate pore size, CdS films of different thickness (200÷1000nm) and morphology were deposited from solution.The electrochemical deposition of $Zn_xCd_{1-x}O$ films with a varied Zn content was performed in a three-electrode configuration: pure graphite, Ag/AgCl and *c*-Si/PS/CdS substrates were used as anode, reference electrode and cathode, respectively. For SEM, XRD, energy dispersive X-ray spectroscopy (EDS) and optical measurements, samples were prepared on glass/$SnO_2$ substrates. Electrodeposition was performed in aqueous solutions of $Zn(NO_3)_2$ and $Cd(NO_3)_2$ (99.5% salt purity). The $Zn_xCd_{1-x}O$ formation potentials were determined in a cyclic voltammetry experiment performed in a potential range of -1.6 to +1.6 V. The thickness of electrodeposited $Zn_xCd_{1-x}O$ films was between 100 and 500nm, depending on the reaction time. The actual composition of the films was determined by EDS and the measured values are reported in Table 1.

The heterojunction formation was completed by evaporating an ohmic In (or Cu) electrode with an area of ~0.82÷1cm$^2$ on the $Zn_xCd_{1-x}O$ films and an Al electrode on the side of the *c*-Si wafer.

* E-mail: mhhuseyng@gmail.com

 

Table 1. Atomic percentages of Zn and Cd in electrodeposited $Zn_xCd_{1-x}O$ thin films of 500nm thickness as determined by EDS.

| $Zn_xCd_{1-x}O$ ($x$) | Zn (%) | Cd (%) |
|---|---|---|
| 0.2 | 19.83±0.2% | 80.17±0.4% |
| 0.4 | 40.24±1.2% | 59.76±0.6% |
| 0.5 | 49.94±1.4% | 50.06±0.9% |
| 0.6 | 60.11±1.2% | 39.89±0.4% |

The morphological characterization of the PS and $Zn_xCd_{1-x}O$ films was performed by SEM and AFM. SEM images presented in Figure show the formation of porous silicon with an average pore size of 8÷11nm (PS1) (Fig. 1a); 10÷16nm (PS2) (Fig.1c) and 30÷40nm (PS3) (Fig. 1e), depending on the anodization voltage, current and time.

Figures 1b, d, f show AFM images of $Zn_{0.6}Cd_{0.4}O$ films prepared on *c*-Si/PS/CdS substrates featuring different PS pore sizes. The surface roughness of the films increases with an increasing PS pore diameter. Films deposited on the surface of *c*-Si/PS1/CdS exhibit a homogeneous micro-textured morphology (Fig. 1b). Pyramidal particles are uniformly spread over the surface of *c*-Si/PS2/CdS (Fig. 1d). The $Zn_{0.6}Cd_{0.4}O$ nanocrystallites morphed into spheres as the PS pore diameter increased from 10 to 30 nm. SEM and AFM images indicated that the corresponding grain size increased slightly up to 30÷45nm (Fig. 1f).

X–ray diffraction patterns of $Zn_xCd_{1-x}O$ films deposited on glass/$SnO_2$ substrates (depicted in Fig. 2.) confirm that the $Zn_xCd_{1-x}O$ ternary alloys possess a hexagonal wurtzite structure. All deposited films have a polycrystalline structure with a strongly preferred (002) c-axis orientation (as evidenced by the high intensity of the (002) diffraction peak). The d-spacing values obtained match those of the corresponding reference material (Joint Committee on Powder Diffraction Standard card No. 36-1451) well.

Transmission spectra of $Zn_xCd_{1-x}O$ films (with thickness of 500nm) with a different Zn content are shown in Fig. 3. The maximum transmittance of the films at 556nm, increased from 56% to 89% above the fundamental absorption edge with increasing Zn contents. The transmittance spectra of the films features a sharp absorption edge that shifts towards shorter wavelengths with increasing Zn concentration. The bandgaps of $Zn_xCd_{1-x}O$ films were determined by extrapolating the straight line section of the $(\alpha h\nu)^2$ versus $h\nu$ curves. Bandgap values were found to decrease linearly from 2.95eV ($x$=0.6) to 2.64eV ($x$=0.2) as a function of Zn concentration [18, 19].

The photoelectrical properties of *c*-Si/PS/CdS/$Zn_xCd_{1-x}O$ heterojunctions were investigated as functions of the PS pore size and the Zn content ($x$) of the $Zn_xCd_{1-x}O$ films.

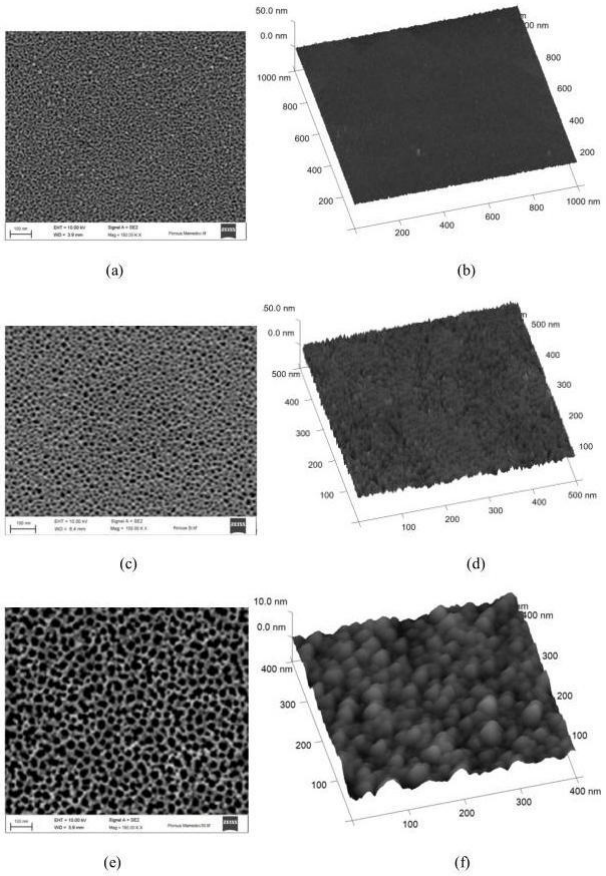


Fig. 1. SEM images (a), (c), (e) of PS1, PS2 and PS3; AFM images of $Zn_{0.6}Cd_{0.4}O$ films deposited on *c*-Si/PS/CdS substrates.

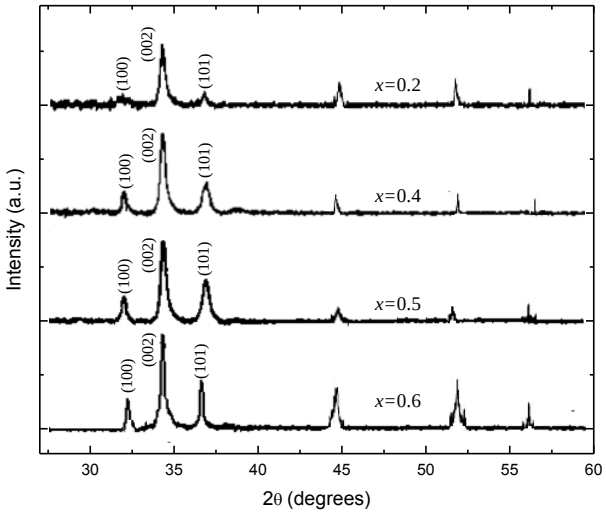


Fig. 2. X–ray diffraction patterns for $Zn_xCd_{1-x}O$films deposited on *c*-Si/PS2/CdS substrates with different $x$.

 

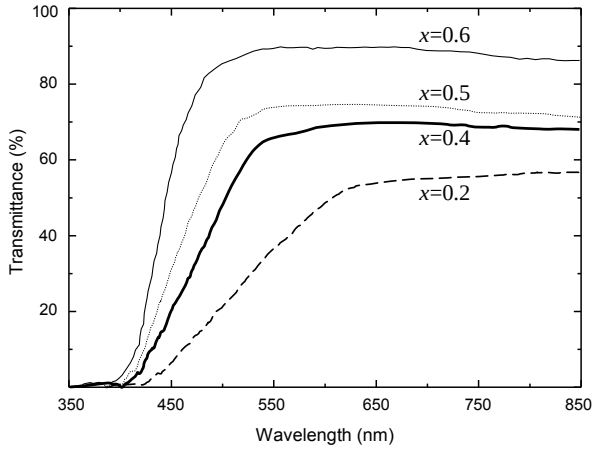


Fig. 3. Transmission spectra of the films $Zn_xCd_{1-x}O$ with a different Zn content.

The *c*-Si/PS/CdS heterojunctions with embedded 150nm thick $Zn_xCd_{1-x}O$ layers exhibit the best overall photoelectrical characteristics. With increasing *x*, the short wavelength peak experienced a blue-shift due to the increased band gap of $Zn_xCd_{1-x}O$. At *x*=0.6, the peak is observed at 420nm.

The spectral dependences of a photocurrent in structures *c*-Si/PS/CdS/$Zn_{0.6}Cd_{0.4}O$ based on PS1, PS2 and PS3 are shown in Fig. 4. It is evident that a minor increase in pore size results in a sharp increase of photosensitivity in all spectral regions. This behavior is characteristically different from that observed earlier in heterojunctions of c-Si/$A_2B_6$ [20, 21], therefore, it can be attributed to light absorption in porous silicon. Heterojunctions based on PS2 exhibit larger efficiency compared to those based on PS1 and PS3 (Tables 2 and 3).

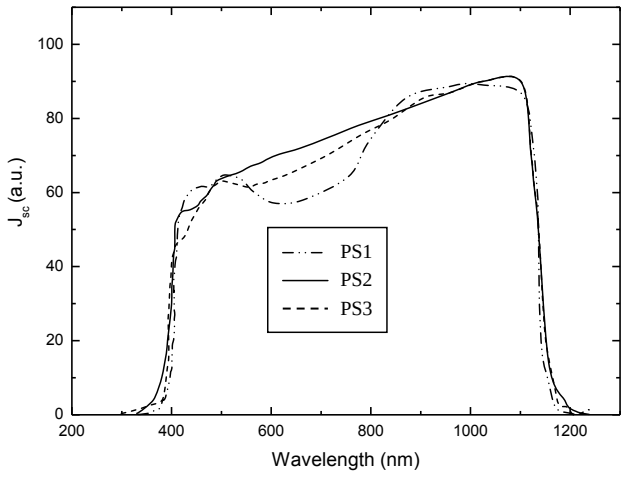


Fig. 4. Spectral dependences of a photocurrent in structures *c*-Si/PS/CdS/$Zn_{0.6}Cd_{0.4}O$ with PS1, PS2 and PS3.

This can be tentatively attributed to the loss of performance due to the structural defects in the polycrystalline film [22, 23]. Although it is true that the efficiency obtained by us is comparatively small for silicon solar cells, but the heterojunctions we obtained on the basis of a simple and cheap method, electrochemical deposition, broadens the prospects of these heterojunctions.

Table 2. Photoelectrical parameters of heterojunctions *c*-Si/PS1/CdS/ $Zn_xCd_{1-x}O$ depending on the Zn content.

| Zn content (*x*) | $U_{oc}$ (mV) | $J_{sc}$ (mA/cm$^2$) | FF | η, % |
|---|---|---|---|---|
| *Samples without ZnCdO* | 482 | 15.7 | 0.53 | 4.01 |
| 0.2 | 504 | 15.3 | 0.53 | 4.09 |
| 0.4 | 513 | 15.1 | 0.53 | 4.1 |
| 0.5 | 527 | 14.9 | 0.54 | 4.24 |
| 0.6 | 543 | 14.6 | 0.54 | 4.28 |

Table 3. Photoelectrical parameters of heterojunctions *c*-Si/PS/CdS/ $Zn_{0.6}Cd_{0.4}O$ with PS1, PS2 and PS3.

| Porous silicon | $U_{oc}$ (mV) | $J_{sc}$ (mA/cm$^2$) | FF | η, % |
|---|---|---|---|---|
| PS1 (*samples with ZnCdO*) | 543 | 14.6 | 0.54 | 4.28 |
| PS2 (*samples without ZnCdO*) | 557 | 21.3 | 0.65 | 7.71 |
| PS2 (*samples with ZnCdO*) | 602 | 23.8 | 0.69 | 9.89 |
| PS3 (*samples with ZnCdO*) | 592 | 19.8 | 0.61 | 7.15 |

## References


[1] M.A. Green, Progress in Photovoltaic **7**, 327 (1999).
[2] P. Papet, O. Nichiporik, A. Kaminski *et al.*, Solar Ener. Mat. Solar Cells **90**, 2319 (2006).
[3] P. Vitanovet *et al.*, Thin Solid Films **297**, 299 (1997).
[4] L. Santinacci *et al.*, Electrochim. Acta **56**, 878 (2010).
[5] V. Lehmann, J. Electrochem. Soc. **140**, 2836 (1993).
[6] O. Bisi *et al.*, Surface Science Reports **38**, 1 (2000).
[7] A.I. Raid *et al.*, Appl. Nanoscience **7**, 9 (2016).
[8] M.A. Naser *et al.*, Procedia Engineering **53**, 393 (2013).
[9] D.H. Oha *et al.*, J. Ceram. Process. Res. **9**, 57 (2008).
[10] H. Foll *et al.*, Materials Scien. Eng. **280**, 1 (2002).
[11] P. Granitzer *et al*., Materials **3**, 943 (2010).
[12] G. Korotcenkov, *Porous Silicon: From Formation to Application* (Taylor and Francis Group, CRC Press, Boca Raton, USA 2016).
[13] V.Y. Yerokhov. Renewable Sustain. Energy Rev. **3**, 291 (1999).
[14] A. Ramizy *et al.*, Appl. Surf. Science **257**, 6112 (2011).
[15] F. Ruske *et al.*, Thin Solid Films **515**, 8695 (2007).
[16] Y. Alivov *et al.*, Appl. Phys. Lett. **83**, 2943 (2003).
[17] G.V. Lashkarev *et al.*, Low Temp. Phys. **37**, 289 (2011).
[18] P.M. Devshette *et al*., J. Alloys Compounds **463**, 576 (2008).
[19] Y. Caglar *et al.*, J. Phys. D: Appl. Phys. **42**, 065421 (2009).
[20] A. Abdinov *et al.*, Thin Solid Films **480-481**, 388 (2005).
[21] A. Abdinov *et al.*, Thin Solid Films **511-512**,140 (2006).
[22] J.B. Orhan *et al.*, Sol. Cells **140**, 344 (2015).
[23] H.Ch. Alan *et al.*, J. Photon. Energy **7**, 027001 (2017).


 